European Radiology (2019) 29:1133–1143
https://doi.org/10.1007/s00330-018-5664-z

UROGENITAL

Diagnosis of transition zone prostate cancer using T2-weighted (T2W) MRI: comparison of subjective features and quantitative shape analysis

Satheesh Krishna[1] · Nicola Schieda[2] · Matthew DF McInnes[1] · Trevor A. Flood[3] · Rebecca E. Thornhill[1]

Received: 6 January 2018 / Revised: 3 July 2018 / Accepted: 13 July 2018 / Published online: 13 August 2018
© European Society of Radiology 2018

Abstract

Purpose To assess T2-weighted (T2W) MRI to differentiate transition zone (TZ) prostate cancer (PCa) from benign prostatic hyperplasia (BPH).

Materials and methods With IRB approval, 22 consecutive TZ PCa were retrospectively compared with 30 consecutive BPH (15 stromal, 15 glandular) nodules diagnosed using radical prostatectomy MRI maps. Two blinded radiologists (R1/R2) subjectively assessed the shape (round/oval vs. lenticular) and margin (circumscribed vs. blurred/indistinct) and for a T2W hypointense rim. Both radiologists segmented lesions extracting quantitative shape features (circularity, convexity and topology/skeletal branching). Statistical tests were performed using chi-square (subjective features), Mann-Whitney U (quantitative features), Cohen's kappa/Bland-Altman and receiver-operator characteristic analysis.

Results There were differences in the subjective analysis of the shape, margin and absence of a T2W-rim comparing TZ PCa with BPH ($p < 0.0001$) with moderate to almost perfect agreement [kappa = 0.56 (shape), 0.72 (margin), 0.97 (T2W-rim)]. Area under the curve (AUC ± standard error) for diagnosis of TZ PCas was shape = 0.88 ± 0.05, margin = 0.89 ± 0.04, and T2W-rim = 0.91 ± 0.04. Shape, judged subjectively, was specific (100%/94% R1/R2) with low-to-moderate sensitivity (55%/88% R1/R2). Circularity and convexity differed between groups ($p < 0.001$) with no difference in topology/skeletal branches ($p = 0.31$). Agreement in measurements was substantial for significant quantitative variables and AUC ± SE, sensitivity and specificity for diagnosis of TZ PCa were: circularity = 0.98 ± 0.01, 90%/96%; convexity = 0.85 ± 0.06, 68%/97%. AUCs for circularity were higher than for subjective analysis ($p = 0.01$ and 0.26).

Conclusion Subjective analysis of T2W-MRI accurately diagnoses TZ PCa with high accuracy also demonstrated for quantitative shape analysis, which may be useful for future radiogenomic analysis of transition zone tumors.

Key points

- *Presence of a complete T2-weighted hypointense circumscribed rim accurately diagnoses BPH.*
- *Round shape accurately diagnoses BPH and can be assessed quantitatively using circularity.*
- *Lenticular shape accurately diagnoses TZ PCa and can be assessed quantitatively using convexity.*

Keywords Prostate · Benign prostatic hyperplasia · Prostate cancer · Magnetic resonance imaging · Medical imaging

✉ Nicola Schieda
nschieda@toh.on.ca

[1] Department of Medical Imaging, The Ottawa Hospital, The University of Ottawa, Ottawa, Ontario, Canada

[2] The Ottawa Hospital, The University of Ottawa, 1053 Carling Avenue, Ottawa, Ontario K1Y 4E9, Canada

[3] Department of Anatomical Pathology, The Ottawa Hospital, The University of Ottawa, Ottawa, Ontario, Canada

Abbreviations

AS	Active surveillance
AUC	Area under the curve
BPH	Benign prostatic hyperplasia
DCE	Dynamic contrast enhanced
DICOM	Digital Imaging and Communications in Medicine
DWI	Diffusion weighted imaging
GU	Urogenital
IQR	Interquartile range
MRI	Magnetic resonance imaging

PACS	Picture archiving and communication system
PCa	Prostate cancer
PI-RADS v2	Prostate Imaging Reporting and Data System – version 2
PZ	Peripheral zone
ROC	Receiver-operator characteristic
RP	Radical prostatectomy
T2W	T2 weighted
TRUS	Trans-rectal ultrasound
TZ	Transition zone

Introduction

Transition zone (TZ) prostate cancer (PCa) represents up to 30% of all PCas [1, 2]. TZ tumors are problematic clinically because they are often under-sampled, or not sampled at all, at non-targeted trans-rectal ultrasound (TRUS)-guided template biopsy [3]. TZ cancers are a leading cause of failure of active surveillance (AS) and are a main source of occult tumors in men with previously negative template TRUS-guided biopsy and subsequent clinically significant (Gleason score ≥ 7) PCa diagnosis [4, 5]. Multiparametric (mp) MRI (T2-weighted [T2W] MRI + diffusion-weighted imaging [DWI] + dynamic contrast enhanced [DCE] MRI [6, 7]) is highly accurate for the detection of clinically significant tumors [8, 9]. mp-MRI is particularly valuable for the diagnosis of TZ cancers and has become the standard of care in men with previously negative TRUS-guided template biopsy with high clinical suspicion of cancer and in men being considered for or being treated with AS [10, 11].

A limitation of mp-MRI for the diagnosis of TZ PCa is the potential for overlap of imaging features with benign prostatic hyperplasia (BPH) nodules, which are ubiquitous in the TZ of adult men [12, 13]. It has been demonstrated that findings on DCE overlap between TZ PCa and BPH [14, 15], and DCE is no longer considered valuable for assessment of the TZ in the updated Prostate Imaging Reporting and Data System (PI-RADS) version 2 (v2) guidelines [16, 17]. DWI is the key (determining) MRI sequence for diagnosis of peripheral zone (PZ) PCa on mp-MRI using PI-RADS v2 [16, 17]; however, there is an overlap of apparent diffusion coefficient (ADC) values comparing TZ PCa and stromal BPH on DWI [18]. Accordingly, PI-RADS v2 suggests that T2W-MRI should be used as the determining sequence for evaluation of the TZ [16, 17]. Features strongly favoring the diagnosis of PCa as reported in PI-RADS v2 are: homogeneously hypointense, lenticular shape, non-circumscribed (or non-encapsulated) with blurred or indistinct margins (smudged or smeared border) and lack of a T2W hypointense rim [16, 17].

The described imaging findings of TZ cancer on T2W-MRI in PI-RADS v2 are subjective and may not be entirely reproducible; for this reason, the use of quantitative analysis of T2W imaging features may be of value. For example, quantitative texture analysis of MRI has previously been shown to successfully distinguish TZ PCa from BPH nodules [19]. Furthermore, it has been demonstrated that texture analysis can improve interobserver agreement relative to subjective evaluation of tumor texture [20–22]. To our knowledge, no previous investigations have evaluated the quantitative analysis of shape features in TZ PCa. It is important to validate these novel features, particularly if they can be ultimately incorporated into future radiogenomic tools for PCa diagnosis. The purpose of our study is therefore to compare the subjective analysis of shape features on T2W-MRI to quantitative shape analysis for diagnosis of TZ PCa.

Materials and methods

Patients

This retrospective study was approved by our local research ethics board, which waived the need for informed consent in all patients. From an existing database of 156 patients who underwent radical prostatectomy (RP) and preoperative mp-MRI of the prostate at 3 T with whole-mount histopathology mp-MRI maps created between May 2012 and May 2015, we created a case-control study group consisting of TZ tumors and BPH nodules. All patients in the cohort had clinically significant cancers that necessitated RP. Those patients, that formed the control group of BPH nodules had purely PZ tumors on whole-mount histopathology mp-MRI maps with no areas of TZ cancer. A flow diagram of patient selection with inclusion and exclusion criteria is provided in Fig. 1.

MRI technique

The multiparametric (T2W + DWI + DCE) MRI technique used for prostate cancer imaging at our institution is provided in Table 1. Endorectal coils were not utilized in any patients.

Histopathology and reference standard

RP specimens were fixed in 40% buffered formalin then serially sectioned into horizontal sections of 0.3 – 0.4 cm thickness using a step-by-step approach. All tissues were paraffin-embedded, and 4-μ-thick sections were cut followed by staining with hematoxylin and eosin. All RP specimen results were reviewed by a fellowship-trained urogenital (GU) pathologist (TAF) with 12 years of experience in GU pathology. Potentially clinically significant tumor foci within each RP specimen were identified. The dominant tumor foci were defined as measuring at least 0.5 ml in size [23–27], and tumors in the PZ and TZ were identified.

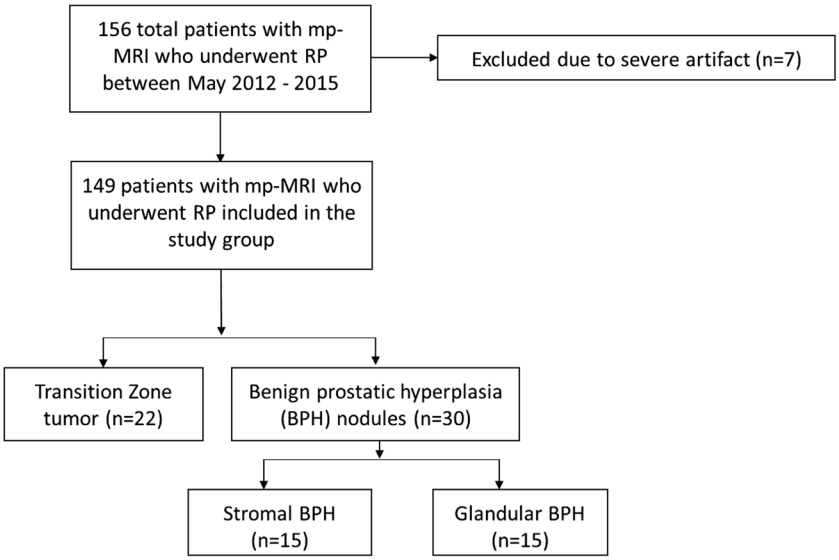

Fig. 1 Flow diagram for patient selection used in this consecutive retrospective study. mp-MRI = Multiparametric MRI; RP = radical prostatectomy

Using existing whole-mount histopathology mp-MRI maps (which were created using RP-mp-MRI registration described previously [28, 29]), a fellowship-trained radiologist identified the clinically significant tumor foci located predominantly (defined as > 2/3 of tumor bulk) in the TZ of the prostate. The transition zone was defined as tissue around the urethra separated from the peripheral zone by a 'surgical capsule' delineated as a low signal line on T2W-MRI [17]. Twenty-two TZ tumors were identified in 22 patients, and the sample was one of convenience. The TZ cancers had been previously investigated by our group with mp-MRI for diagnosis of extraprostatic extension [28] but no features pertaining to the current study have been previously reported.

The control group was created by consecutively identifying 30 BPH nodules (15 glandular BPH and 15 stromal BPH nodules) in 26 patients. All patients in the control group had clinically significant PZ cancers but no evidence of cancer in the TZ at RP. The criteria for selection of a BPH nodule have been described previously [14, 30] but consisted mainly of a localized lesion/mass in the TZ corresponding to an area of BPH on histopathology. Since the vast majority of BPH nodules show mixed glandular and stromal features at histopathology [31], in this study, a stromal BPH nodule was diagnosed when it showed > 90% iso- to hypointense signal on T2W compared with the anterior fibromuscular stroma, and a glandular BPH nodule was required to show > 90% iso- to hyperintensity on T2W compared with the adjacent normal PZ. In this fashion, 30 BPH nodules in 26 patients were identified. Mean patient age (± standard deviation [SD]) was 65.4 ±6.1 with no difference comparing the TZ PCa and BPH groups ($p = 0.57$). We selected 30 BPH nodules as the control group *a priori* to approximate the number of TZ cancers in our study. We did not specifically perform a power analysis to create our control group because of the ubiquitous nature of BPH in adult men and the necessity to use patients with PZ cancers to form the BPH group (because of the requirement of histologic confirmation of absence of cancer in the TZ). The number of control BPH nodules in our study is roughly concordant with what has been previously reported in the literature when assessing BPH and TZ PCa with MRI [32, 33].

Subjective analysis

Two fellowship-trained abdominal radiologists with 6 and 12 years of experience in GU radiology (SK and NS), both experienced with the PI-RADS v2 system (each having interpreted > 200 examinations using PI-RADS v2), evaluated MR examinations independently and blinded to the final histopathology results. Radiologists were provided with the location of masses on T2W-MRI using a PI-RADS v2 sector map. All MR images were available at the time of imaging review (including T2W, DWI and DCE); however, for the purpose of this study only T2W-MRI was specifically evaluated. Each examination was reviewed on a standard PACS (Horizon Medical Imaging, McKesson Corp., San Francisco CA) workstation.

Radiologists evaluated for the following imaging features on T2W-MRI as described in PI-RADS v2: shape (round or oval versus lenticular), margin (circumscribed [smooth or lobulated] versus non-circumscribed [blurred, indistinct, irregular or spiculated]) and presence or absence of a complete hypointense rim (Figs. 2, 3, and 4).

Quantitative analysis

At the time of subjective imaging review, each radiologist also independently segmented lesions to enable quantitative shape analysis. Patient-identifying information was removed, and the axial T2W-MRI image that depicted the

Table 1 Sequence parameters for multiparametric MRI of the prostate protocol performed with pelvic surface coil[a] at 3 T[b]

	Imaging plane	Field of view (mm)	Matrix size	Slice thickness/gap (mm)	TR/TE (ms)	Echo train length	Flip angle	Acceleration factor	Receiver bandwidth (Hz/voxel)	Acquisition time (min)	Number of signals averaged
T1 TSE[c]	Axial	350 × 350	320 × 320	5.0/1.0	720/8-14	3	111	N/A	244	4 min	2
T1 3D Dual Echo GRE[d]	Axial	240 × 240	292 × 224	4.0/1.0	4.8/1.1-1.3;TE12.2-2.5; TE2	N/A	12	2	558	Breath hold	1
T2 TSE	Coronal Sagittal Axial	220 × 220	320 × 256	4.0/0 3.0/0 3.0/0	3890-5250/105-125	27-35	111	N/A	122	4 min 4 min 4 min	1-2
DWI[e]	Axial	280 × 280	128 × 80	3-5.0/0	4200/90	1	90	2	1950	5 min	4-10
T1 GRE[f] dynamic contrast	Axial	220 × 220	128 × 128	4.0/0	4.3/1.3	N/A	12	2	488	6 min	1

[a] Integrated pelvic surface coils (4–16 channels) with activated spine coils (8-12 channels)

[b] Clinical 3-T systems: TRIO TIM (Siemens Medical, Malvern PA) and Discovery 750W (General Electric, Milwaukee WI)

[c] Turbo/fast spin echo

[d] Gradient recalled echo

[e] DWI = Diffusion-weighted imaging performed with spectral fat-suppression echo planar imaging with tridirectional motion probing gradients and B values of 0, 500, 1000 with automatic apparent diffusion coefficient map generation

[f] Dynamic fast spoiled 2D GRE performed with a temporal resolution of 10 s after injection of 0.1 mmol/kg of gadobutrol (Gadovist, Bayer Inc. Toronto, ON) at a rate of 3 ml/s

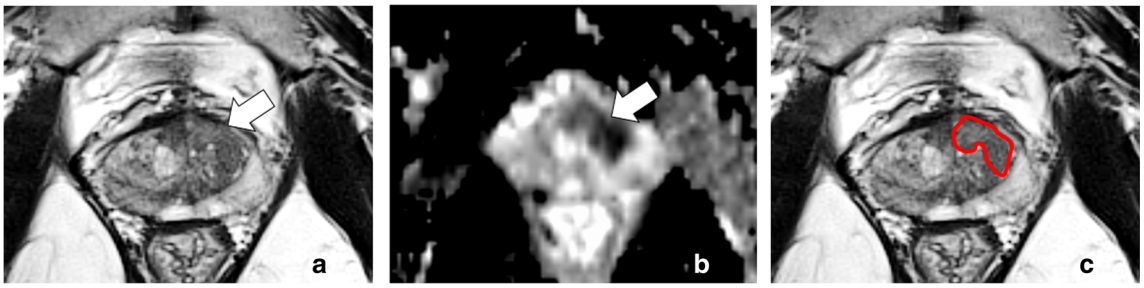

Fig. 2 A 62-year-old male with left transitional zone prostate cancer (TZ PCa). Axial T2-weighted (T2W) (**a**) and apparent diffusion coefficient (ADC) map (**b**) images show lenticular homogeneously low T2W signal intensity lesion in the left TZ (white arrow) with markedly low signal on the ADC map (white arrow). This nodule was characterized as having 'lenticular shape,' 'absence of a T2 hypointense rim' and a 'non-circumscribed margin' by both readers. Axial T2W image (**c**) shows the method of contouring of the lesion for quantitative analysis in this study

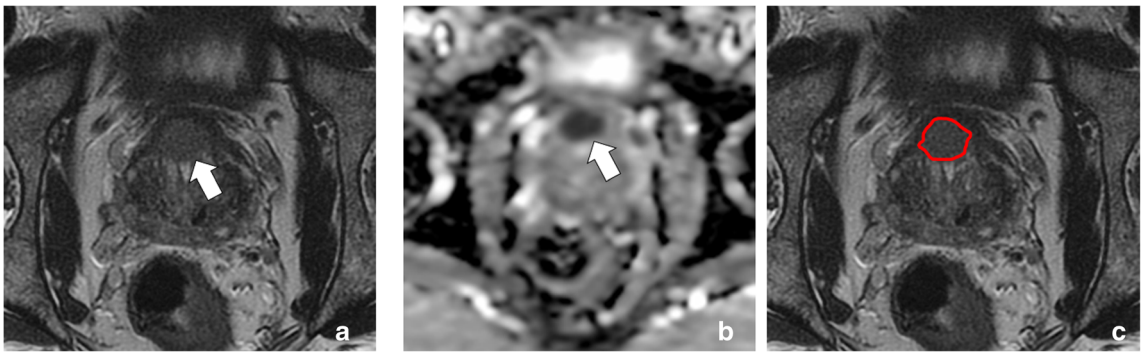

Fig. 3 A 68-year-old male with midline TZ PCa. Axial T2W (**a**) and ADC map (**b**) images show a round homogeneously low T2 signal lesion in the middle TZ (white arrow) with markedly low signal on the ADC map (white arrow). The lesion was characterized as having a 'round shape,' 'absence of T2 hypointense rim' and a 'non-circumscribed margin' by both readers. T2W image (**c**) shows contouring of the lesion for quantitative analysis

mass where it appeared the largest was selected and exported in the DICOM format from PACS to an independent workstation for lesion segmentation using Image J (version 1.48, National Institutes of Health). The radiologists were instructed to manually draw a line along the outer contour of each nodule with a measurement tool and then save their contours as regions of interest (ROIs), which were exported for analysis in random fashion. Segmentation of each tumor required less than 1 min to perform using Image J; however, anonymization of images in DICOM format and transfer to a separate workstation for segmentation were somewhat labor-intensive to perform over the entire population.

For this study, three quantitative shape features were selected *a priori* to approximate the subjective features of TZ PCa and BPH described in PI-RADS v2, namely: (1) circularity, (2) convexity and (3) topology or the number of skeleton branches [34, 35]. The 'circularity'

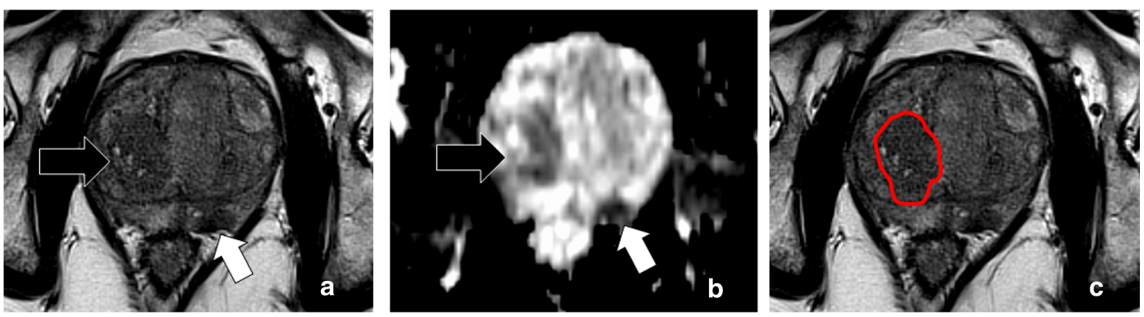

Fig. 4 A 52-year-old male with radical prostatectomy performed for left middle PZ cancer and with extensive BPH. Axial T2W (**a**) and ADC map (**b**) images show the tumor in the left PZ (white arrows). A characteristic stromal BPH nodule in the right TZ shows heterogeneous but predominantly low T2W signal intensity and moderately low signal on the ADC map (black arrows). Note that the low T2W signal rim is absent in (**a**). This nodule was characterized as having a 'round shape,' 'absence of a T2 hypointense rim' and a 'non-circumscribed margin' by both readers. Axial T2W image (**c**) shows the method of contouring of the BPH nodule

Table 2 Subjective assessment of T2-weighted (T2W) MRI features for diagnosis of transition zone (TZ) prostate cancer (PCa) compared with benign prostatic hyperplasia (BPH) nodules

	Radiologist 1			Radiologist 2			
	TZ PCa (n = 22)	BPH (n = 30)	p value[a]	TZ PCa (n = 22)	BPH (n = 30)	p value	Kappa[b]
Lenticular shape	10	0	<0.0001	18	2	<0.0001	0.56
Non-circumscribed margin (blurred, indistinct, spiculated or irregular)	18	1	<0.0001	20	4	<0.0001	0.72
Presence of T2W hypointense rim	1	26	<0.0001	2	27	<0.0001	0.97

[a] Comparisons were performed between groups using the chi-square test

[b] Interobserver agreement assessed using Cohen's kappa statistic

feature is a quantitative descriptor of lesion 'roundedness,' whereas the 'convexity' feature reflects the degree to which the lesion is 'lentiform' with respect to shape. These two quantitative features were selected because they represent the quantitative surrogates of the subjective shape parameters of round versus lenticular in PI-RADS v2. Circularity was defined as $2\sqrt{(A/\pi)}/\sum(D/\pi)$ and convexity as $\sum D$/(convex perimeter), where 'A' denoted the lesion area and D denoted the shape-specific profile perimeter [35]. Topology or the number of skeleton branches is a quantitative indicator of the degree to which the lesion has a 'spiculated' margin [34], and it was selected to assess the subjective parameter of the tumor margin in PI-RADS v2. These quantitative features were computed by a PhD with 15 years of experience in quantitative MRI analysis, blinded to the final diagnosis of each lesion using MaZda version 4.6 (Institute of Electronics, Technical University of Lodz, Poland) [36]. Extraction of features was not time consuming, however required manual transfer of contoured anonymized DICOM images performed in Image J into MaZda for analysis, which can be labor intensive. Most of these labor-intensive manual processes are expected to be simplified and automated in the future.

Statistical analysis

Lesion size is presented as mean ± SD (interquartile range [IQR]) and quantitative shape features (which were non-normally distributed) as median [IQR], respectively. Lesion size and age were compared by independent t-tests and skewed data for quantitative shape features by using the Mann-Whitney U test. Subjective variables were tabulated and compared using the chi-square test. Receiver-operator characteristic (ROC) curves were generated and the area under curve (AUC) reported with the sensitivity and specificity for diagnosis of TZ PCa (using the method of Youden to determine the criterion that corresponded to the maximum accuracy for parametric data). Comparisons of overall accuracy between different variables for diagnosis of BPH versus TZ PCa were performed using ROC analyses. Interobserver agreement was assessed using Cohen's kappa statistic and Bland-Altman analysis for

Table 3 Area under receiver-operator characteristic (ROC) curve analysis and diagnostic accuracy for subjective assessment of T2-weighted (T2W) MRI features for diagnosis of transition zone (TZ) prostate cancer (PCa) compared with benign prostatic hyperplasia (BPH) nodules

	Radiologist 1			Radiologist 2		
	Area under ROC curve (± SE)	Sensitivity (confidence Intervals)	Specificity (confidence Intervals)	Area under ROC curve (± SE)	Sensitivity (confidence intervals)	Specificity (confidence intervals)
Lenticular shape	0.77 (0.05)	54.55% (32.21-75.61%)	100.00% (88.43-100.00%)	0.88 (0.05)	81.82% (59.72-94.81%)	93.33% (77.93-99.18%)
Non-circumscribed margin (blurred, indistinct, spiculated or irregular)	0.89 (0.05)	81.82% (59.72-94.81%)	96.67% (82.78-99.92%)	0.89 (0.04)	83.33% (62.62-95.26%)	92.86% (76.50-99.12%)
Absence of T2W hypointense rim	0.91 (0.04)	86.67% (69.28-96.24%)	95.45% (77.16-99.88%)	0.90 (0.04)	90.00% (73.47-97.89%)	90.91% (70.84-98.88%)

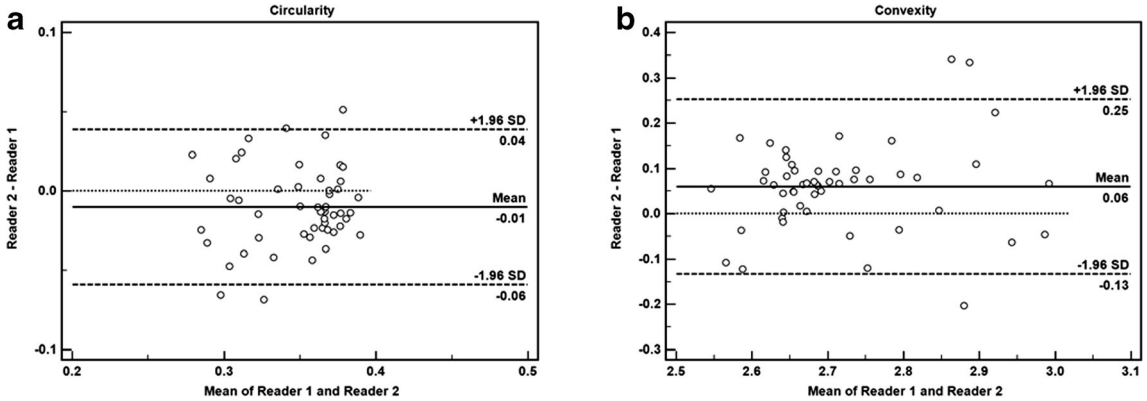

Fig. 5 Bland-Altman plots for circularity (**a**) and convexity (**b**) show low mean difference between the two readers

subjective and quantitative features, respectively. $P < 0.05$ indicated a statistically significant outcome.

Results

TZ tumors measured 18.7 ± 7.7 [IQR 14-24] mm compared to BPH nodules, which measured 17.7 ± 6.4 [IQR 13-20] mm with no difference between groups ($p = 0.6425$).

A summary of subjective assessments performed by both radiologists is provided in Table 2. Subjective assessment of lesion shape (lenticular compared with round/oval), margin (blurred, indistinct, irregular or spiculated compared with circumscribed) and absence of a T2W hypointense rim were all strongly associated with TZ PCa ($p < 0.0001$) for both radiologists. Interobserver agreement was moderate for subjective shape (K = 0.56) and margin (K = 0.72) and almost perfect for T2W hypointense rim (K = 0.97). Area under curve (± standard error [SE]) with sensitivity and specificity (confidence intervals) for diagnosis of TZ PCa are provided in Table 3. All three features showed good degrees of accuracy for diagnosis of TZ PCa with high specificity. Among the three features studied, subjective shape yielded the lowest sensitivity; 54.6% (confidence intervals [CI] 32.21% - 75.61%) for radiologist 1 and 81.8% (59.72% - 94.81%) for radiologist 2.

With respect to quantitative shape features, Bland-Altman analysis of features derived from contours provided by both radiologists demonstrated low mean difference (Fig. 5), and results for both radiologists are summarized in Table 4. Circularity and convexity differed significantly comparing TZ PCa and BPH nodules ($p < 0.0001$). Both features were accurate for differentiating TZ PCa from BPH with AUC (± SE), as summarized in Table 5. Conversely, the lesion topology (number of skeleton branches) associated with TZ PCa did not differ significantly from that of BPH (4.5 [2.0-6.0] vs. 4.5 [3.0-6.0], $p = 0.31$) and did not accurately differentiate TZ PCa from BPH. Comparisons of AUC for subjective and quantitative features are summarized in Table 6. There was a modest improvement in AUC comparing the quantitative shape feature circularity with subjective analyses; however, the difference was only significant for reader 2 ($p = 0.26$ reader 1 and 0.01 reader 2). There was no significant difference in AUC comparing the quantitative shape feature convexity to subjective analysis for either reader ($p = 0.38$ and 0.65, Reader 1 and 2 respectively) (Fig. 6).

Discussion

This study assessed the ability of both subjective and quantitative findings on T2W-MRI to differentiate transition zone prostate cancer from BPH. Our results indicate that lenticular shape, non-circumscribed margin and absence of a T2W hypointense rim are all accurate subjective findings of TZ

Table 4 Quantitative assessment of T2-weighted (T2W) MRI features for diagnosis of transition zone (TZ) prostate cancer (PCa) compared with benign prostatic hyperplasia (BPH) nodules. Results are displayed as median (interquartile range)

	Radiologist 1			Radiologist 2		
	TZ PCa ($n = 22$)	BPH ($n = 30$)	p value[a]	TZ PCa ($n = 22$)	BPH ($n = 30$)	p value
Circularity	0.33 (0.30-0.34)	0.37 (0.37-0.38)	<0.0001	0.31 (0.29-0.35)	0.36 (0.36-0.37)	<0.0001
Convexity	2.75 (0.65-2.84)	2.64 (2.60-2.66)	<0.0001	2.82 (2.72-2.95)	2.69 (2.66-2.72)	<0.0001
Topology	6.5 (4-8)	6.5 (5-8)	0.31	7.5 (5-11)	6 (5-8)	0.30

[a] Comparisons were performed between groups using the Mann-Whitney U test

Table 5 Area under receiver-operator characteristic (ROC) curve analysis and diagnostic accuracy for quantitative assessment of T2-weighted (T2W) MRI features for diagnosis of transition zone (TZ) prostate cancer (PCa) compared with benign prostatic hyperplasia (BPH) nodules

	Radiologist 1			Radiologist 2		
	Area under ROC curve (± SE)	Sensitivity (confidence intervals)	Specificity (confidence intervals)	Area under ROC curve (± SE)	Sensitivity (confidence intervals)	Specificity (confidence intervals)
Circularity	0.98 (0.01)	90.52% (73.52-97.96)	95.5% (77.22-99.99)	0.85 (0.07)	96.72% (82.81-99.99)	72.71% (45.13-86.14)
Convexity	0.85 (0.06)	68.22% (45.11-86.13)	100.0% (88.42-100.00)	0.84 (0.07)	68.22% (45.12-86.13)	96.74% (82.82-99.99)
Topology	0.58 (0.08)	18.32% (6.45-42.56)	100.00% (72.34-100.00)	0.58 (0.08)	41.34% (22.45-64.42)	77.56% (42.65-93.56)

cancer and show moderate to almost perfect levels of interobserver agreement. Quantitatively, circularity and convexity shape features also accurately differentiated TZ PCa and BPH with excellent interreader agreement; however, the quantitative feature related to lesion topology (number of skeleton branches) was not capable of differentiating between TZ PCa and BPH, demonstrating inferior accuracy to subjective assessment of the tumor margin. Our results are important because they indicate a potential role for quantitative analysis of lesion shape when differentiating between TZ PCa and BPH, which can potentially be incorporated in subsequent larger scale radiogenomic studies that include machine-learning strategies for the diagnosis of TZ PCa.

The subjective results from our study of T2W-MRI to diagnose TZ PCa compare favorably to what has been published in the literature. Akin et al evaluated subjective features of TZ PCa and reported a similar high sensitivity and specificity for 'ill-defined margins' and 'lack of capsule' [37]. The specificity of 'lenticular shape' was high (85-98%), whereas the sensitivity was low (48-56%), which compares favorably with our results [37]. A similar low sensitivity of 30-50% for lenticular shape has also been reported by other investigators [15, 38]. Oto et al differentiated TZ PCa from BPH nodules using subjective morphologic features and also concluded that subjective features were less desirable because of the high degree of overlap with BPH nodules; for example, in their study the sensitivity of 'lenticular shape' for identification of TZ PCa was only 16% [18]. These studies along with results provided in the current study highlight the challenges in accurate categorization of TZ nodules using subjective morphologic descriptors and the need for more reliable quantitative metrics to improve accuracy.

Previously, Sidhu et al used quantitative analysis of textural features to identify TZ PCa [19]. Although previous quantitative studies have revealed differences in shape of the entire prostate gland comparing normal and diseased prostates [39], to our knowledge, we are the first to describe the potential use of quantitative analysis of shape features of lesions in the TZ to diagnose PCa compared with BPH and to compare these features with subjective analysis. Our results indicate that lesion topology (a measure of the number of skeleton branches) was not useful to diagnose TZ PCa and was inferior to the radiologist's subjective evaluation of the lesion margin (including assessment of contour and presence or absence of a T2W hypointense rim). Quantitative analysis of lesion shape using circularity and convexity was accurate for diagnosis of TZ PCa and showed modest improvements in overall accuracy compared with subjective judgment of shape. These results indicate that shape, as a quantitative metric, may prove useful in combination with other previously described quantitative

Table 6 Comparison of area under receiver operator characteristic curve (AUC) for subjective shape analysis and quantitative shape analyses of transition zone prostate cancers compared to BPH nodules

	Circularity[a]	Convexity	Topology
Reader 1			
Shape	0.77 (0.05) vs. 0.98 (0.01)$p = 0.26$	0.77 (0.05) vs. 0.85 (0.07)$p = 0.38$	
Margin			0.89 (0.05) vs. 0.58 (0.08)$p < 0.001$
Rim			0.91 (0.04) vs. 0.58 (0.08)$p < 0.001$
Reader 2			
Shape	0.88 (0.05) vs. 0.85 (0.07)$p = 0.01$	0.88 (0.05) vs. 0.84 (0.07)$p = 0.65$	
Margin			0.89 (0.04) vs. 0.58 (0.08)$p < 0.001$
Rim			0.90 (0.04) vs. 0.58 (0.08)$p < 0.001$

[a] Data are presented as AUC (SE) for subjective features vs. quantitative features

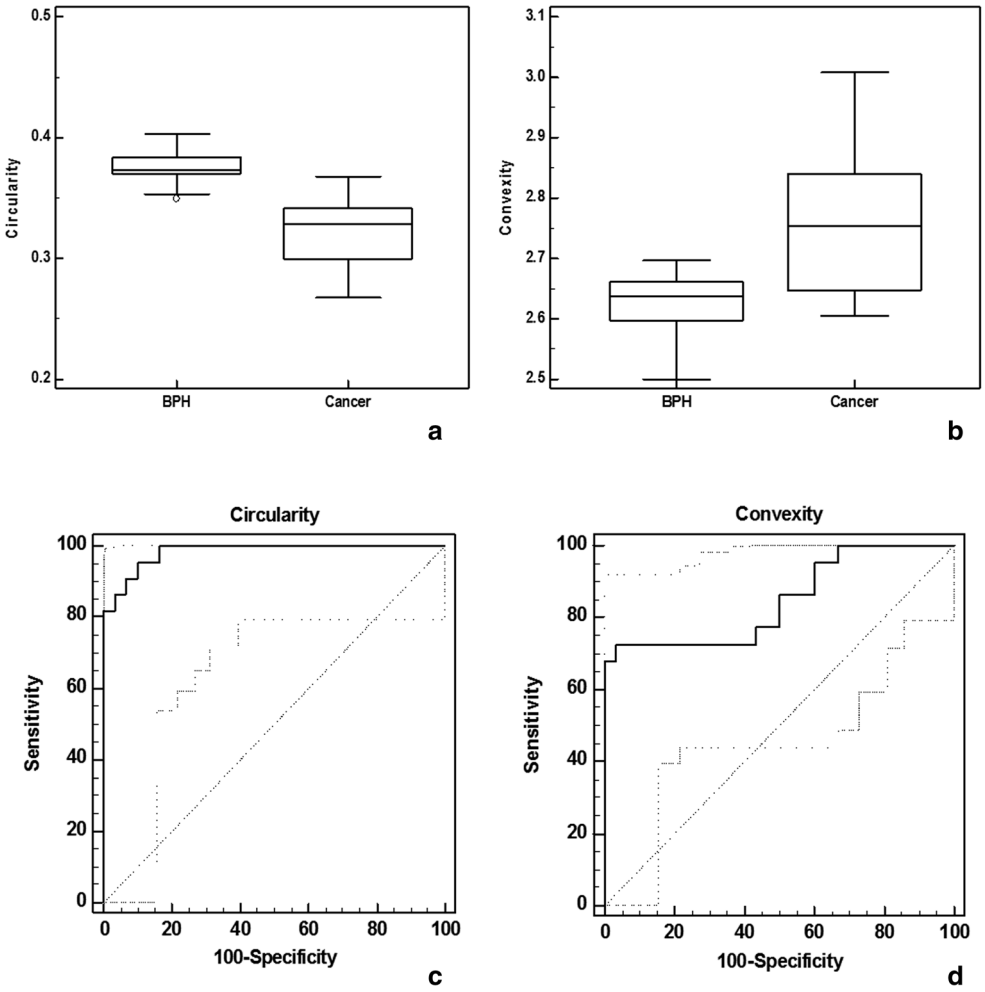

Fig. 6 Box-and-whisker plots comparing circularity (**a**) and convexity (**b**) between BPH and TZ Pca. TZ PCa shows high median convexity and low median circularity compared with BPH nodules. Receiver-operator characteristic (ROC) curves for circularity (**c**) and convexity (**d**) to differentiate between TZ prostate cancer and BPH show an excellent degree of accuracy with high areas under the curve (AUC), which were higher for circularity compared with subjective analysis

imaging features such as texture, ADC analysis and location of a TZ abnormality [15], particularly if carefully incorporated into a large, well-validated machine-learning tool. Future study into this exciting radiomic strategy is required. Preliminary reports have shown promising early results for automated detection of PZ tumors; however, studies evaluating solely the TZ are limited and have shown less favorable results [40, 41]. Shape analysis, in additional to study of other radiomic features, often requires analysis of anonymized DICOM images on separate workstations not integrated into commercial PACS. Though the process of image segmentation and analysis itself are not overly time consuming, workflow for segmentation and analysis (due to lack of integration into PACS) is tedious, and future integration or commercially supported radiomic products could improve utilization in practice.

Our study has limitations. The sample size is relatively small, though comparable to what has been published previously regarding the MRI appearance of TZ PCa and BPH [18, 32, 33]. The single institution study design that necessitated radical prostatectomy for histologic confirmation of cancer and BPH introduces population bias into our results, specifically because BPH nodules were evaluated in patients with known clinically significant cancers of the PZ. We elected not to use targeted biopsy results of TZ nodules that yielded a diagnosis of BPH because of the risk of false-negative diagnosis compared with RP. The use of RP-MRI mapping, which confirmed BPH, and the absence of TZ cancer in the control group helped to mitigate the risk of bias as it is essentially not possible to assess BPH nodules with RP confirmation in patients without a PZ cancer. Since we required RP correlation as the reference standard, all men in our study had a clinically significant cancer that necessitated RP. It is possible that if radiologists identified a PZ cancer at the time of blinded review they may have been biased toward realizing the examination was an example of BPH and conversely the absence of a PZ tumor might suggest the presence of a TZ tumor. Our reported diagnostic accuracies may therefore represent overestimates of what can be expected in clinical practice, especially given that radiologists were also provided with the location of lesions when interpreting MRI, which may artificially increase the sensitivity of diagnosis.

In conclusion, our study demonstrates that quantitative shape analysis is an accurate quantitative metric for diagnosis

of transition zone prostate cancer with strong agreement in measurements and modest improvements in accuracy of diagnosis compared with subjective shape analysis. Comparatively, subjective assessment of the lesion margin (including the presence or absence of a T2W hypointense rim) outperformed quantitative assessment of the margin, which was not useful. Our results show a potential role for quantitative shape analysis of prostate lesions, which when combined with other quantitative metrics may be incorporated into future studies evaluating automated detection of transition zone PCa by machine learning.

Funding The authors state that this work has not received any funding.

Compliance with ethical standards

Guarantor The scientific guarantor of this publication is Nicola Schieda, MD FRCP(C).

Conflict of interest The authors of this manuscript declare no relationships with any companies, whose products or services may be related to the subject matter of the article.

Statistics and biometry No complex statistical methods were necessary for this article. One of the authors, Dr. Rebecca E. Thornhill, provided statistical advice for this manuscript.

Informed consent Written informed consent was waived by the Institutional Review Board.

Ethical approval Institutional Review Board approval was obtained.

Methodology
- retrospective
- case-control study
- performed at one institution

References

1. Haas GP, Sakr WA (1997) Epidemiology of prostate cancer. CA Cancer J Clin 47:273–287
2. Reissigl A, Pointner J, Strasser H, Ennemoser O, Klocker H, Bartsch G (1997) Frequency and clinical significance of transition zone cancer in prostate cancer screening. Prostate 30:130–135
3. Durkan GC, Sheikh N, Johnson P, Hildreth AJ, Greene DR (2002) Improving prostate cancer detection with an extended-core transrectal ultrasonography-guided prostate biopsy protocol. BJU Int 89:33–39
4. Kim K, Lee JK, Choe G, Hong SK (2016) Intraprostatic locations of tumor foci of higher grade missed by diagnostic prostate biopsy among potential candidates for active surveillance. Sci Rep 6:36781
5. Duffield AS, Lee TK, Miyamoto H, Carter HB, Epstein JI (2009) Radical prostatectomy findings in patients in whom active surveillance of prostate cancer fails. J Urol 182:2274–2278
6. Quon JS, Moosavi B, Khanna M, Flood TA, Lim CS, Schieda N (2015) False positive and false negative diagnoses of prostate cancer at multi-parametric prostate MRI in active surveillance. Insights Imaging 6:449–463
7. Hegde JV, Mulkern RV, Panych LP et al (2013) Multiparametric MRI of prostate cancer: an update on state-of-the-art techniques and their performance in detecting and localizing prostate cancer. J Magn Reson Imaging 37:1035–1054
8. de Rooij M, Hamoen EH, Fütterer JJ, Barentsz JO, Rovers MM (2014) Accuracy of multiparametric MRI for prostate cancer detection: a meta-analysis. AJR Am J Roentgenol 202:343–351
9. Fusco R, Sansone M, Granata V, Setola SV, Petrillo A (2017) A systematic review on multiparametric MR imaging in prostate cancer detection. Infect Agent Cancer 12:57
10. Abd-Alazeez M, Ahmed HU, Arya M et al (2014) The accuracy of multiparametric MRI in men with negative biopsy and elevated PSA level–can it rule out clinically significant prostate cancer? Urol Oncol 32(45):e17–e22
11. Barrett T, Haider MA (2017) The emerging role of MRI in prostate cancer active surveillance and ongoing challenges. AJR Am J Roentgenol 208:131–139
12. Hoeks CM, Hambrock T, Yakar D et al (2013) Transition zone prostate cancer: detection and localization with 3-T multiparametric MR imaging. Radiology 266:207–217
13. Rosenkrantz AB, Taneja SS (2014) Radiologist, be aware: ten pitfalls that confound the interpretation of multiparametric prostate MRI. AJR Am J Roentgenol 202:109–120
14. Elbuluk O, Muradyan N, Shih J et al (2016) Differentiating transition zone cancers from benign prostatic hyperplasia by quantitative multiparametric magnetic resonance imaging. J Comput Assist Tomogr 40:218–224
15. Chesnais AL, Niaf E, Bratan F et al (2013) Differentiation of transitional zone prostate cancer from benign hyperplasia nodules: evaluation of discriminant criteria at multiparametric MRI. Clin Radiol 68:e323–e330
16. Barentsz JO, Weinreb JC, Verma S et al (2016) Synopsis of the PI-RADS v2 guidelines for multiparametric prostate magnetic resonance imaging and recommendations for use. Eur Urol 69:41–49
17. Weinreb JC, Barentsz JO, Choyke PL et al (2016) PI-RADS prostate imaging - reporting and data system: 2015, version 2. Eur Urol 69:16–40
18. Oto A, Kayhan A, Jiang Y et al (2010) Prostate cancer: differentiation of central gland cancer from benign prostatic hyperplasia by using diffusion-weighted and dynamic contrast-enhanced MR imaging. Radiology 257:715–723
19. Sidhu HS, Benigno S, Ganeshan B et al (2017) Textural analysis of multiparametric MRI detects transition zone prostate cancer. Eur Radiol 27:2348–2358
20. Rosenkrantz AB, Ginocchio LA, Cornfeld D et al (2016) Interobserver reproducibility of the PI-RADS version 2 lexicon: a multicenter study of six experienced prostate radiologists. Radiology 280:793–804. https://doi.org/10.1148/radiol.2016152542
21. Dinh CV, Steenbergen P, Ghobadi G et al (2016) Magnetic resonance imaging for prostate cancer radiotherapy. Phys Med 32:446–451
22. Niu XK, Chen ZF, Chen L, Li J, Peng T, Li X (2017) Clinical application of biparametric MRI texture analysis for detection and evaluation of high-grade prostate cancer in zone-specific regions. AJR Am J Roentgenol 210:549–556
23. Stamatakis L, Siddiqui MM, Nix JW et al (2013) Accuracy of multiparametric magnetic resonance imaging in confirming eligibility for active surveillance for men with prostate cancer. Cancer 119:3359–3366
24. Montironi R, Hammond EH, Lin DW et al (2014) Consensus statement with recommendations on active surveillance inclusion criteria and definition of progression in men with localized prostate cancer: the critical role of the pathologist. Virchows Arch 465:623–628

25. Turkbey B, Mani H, Aras O et al (2012) Correlation of magnetic resonance imaging tumor volume with histopathology. J Urol 188: 1157–1163
26. Amin MB, Lin DW, Gore JL et al (2014) The critical role of the pathologist in determining eligibility for active surveillance as a management option in patients with prostate cancer: consensus statement with recommendations supported by the College of American Pathologists, International Society of Urological Pathology, Association of Directors of Anatomic and Surgical Pathology, the New Zealand Society of Pathologists, and the Prostate Cancer Foundation. Arch Pathol Lab Med 138:1387–1405
27. Johnson LM, Choyke PL, Figg WD, Turkbey B (2014) The role of MRI in prostate cancer active surveillance. Biomed Res Int 2014: 203906
28. Krishna S, Lim CS, McInnes MDF et al (2017) Evaluation of MRI for diagnosis of extraprostatic extension in prostate cancer. J Magn Reson Imaging. https://doi.org/10.1002/jmri.25729
29. Rozenberg R, Thornhill RE, Flood TA, Hakim SW, Lim C, Schieda N (2016) Whole- tumor quantitative apparent diffusion coefficient histogram and texture analysis to predict gleason score upgrading in intermediate-risk 3 + 4 = 7 prostate cancer. AJR Am J Roentgenol 206:775–782
30. Liu X, Zhou L, Peng W, Wang C, Wang H (2013) Differentiation of central gland prostate cancer from benign prostatic hyperplasia using monoexponential and biexponential diffusion-weighted imaging. Magn Reson Imaging 31:1318–1324
31. Roehrborn CG (2008) Pathology of benign prostatic hyperplasia. Int J Impot Res 20(Suppl 3):S11–S18
32. Schiebler ML, Tomaszewski JE, Bezzi M et al (1989) Prostatic carcinoma and benign prostatic hyperplasia: correlation of high-resolution MR and histopathologic findings. Radiology 172:131–137
33. Bao J, Wang X, Hu C, Hou J, Dong F, Guo L (2017) Differentiation of prostate cancer lesions in the transition zone by diffusion-weighted MRI. Eur J Radiol Open 4:123–128
34. Pena E, Ojiaku M, Inacio JR et al (2017) Can CT and MR shape and textural features differentiate benign versus malignant pleural lesions? Acad Radiol 24:1277–1287
35. Thornhill RE, Lum C, Jaberi A et al (2014) Can shape analysis differentiate free-floating internal carotid artery thrombus from atherosclerotic plaque in patients evaluated with CTA for stroke or transient ischemic attack? Acad Radiol 21:345–354
36. Szczypiński PM, Strzelecki M, Materka A, Klepaczko A (2009) MaZda–a software package for image texture analysis. Comput Methods Programs Biomed 94:66–76
37. Akin O, Sala E, Moskowitz CS et al (2006) Transition zone prostate cancers: features, detection, localization, and staging at endorectal MR imaging. Radiology 239:784–792
38. Lemaitre L, Puech P, Poncelet E et al (2009) Dynamic contrast-enhanced MRI of anterior prostate cancer: morphometric assessment and correlation with radical prostatectomy findings. Eur Radiol 19:470–480
39. Rusu M, Purysko AS, Verma S et al (2017) Computational imaging reveals shape differences between normal and malignant prostates on MRI. Sci Rep 7:41261
40. Dinh AH, Melodelima C, Souchon R et al (2018) Characterization of prostate cancer with Gleason score of at least 7 by using quantitative multiparametric MR imaging: validation of a computer-aided diagnosis system in patients referred for prostate biopsy. Radiology. https://doi.org/10.1148/radiol.2017171265
41. Le MH, Chen J, Wang L et al (2017) Automated diagnosis of prostate cancer in multi-parametric MRI based on multimodal convolutional neural networks. Phys Med Biol 62:6497–6514